Rotational band structures in $N=89$ ^{153}Gd

T. B. Brown,* M. A. Riley, D. Campbell, D. J. Hartley,† F. G. Kondev,‡ and J. Pfohl
Department of Physics, Florida State University, Tallahassee, Florida 32306

R. V. F. Janssens,§ S. M. Fischer,‖ and D. Nisius¶
Argonne National Laboratory, Argonne, Illinois 60439

P. Fallon
Nuclear Science Division, Lawrence Berkeley National Laboratory, Berkeley, California 94720

W. C. Ma
Mississippi State University, Mississippi State, Mississippi 39762

J. Simpson
CLRC, Daresbury Laboratory, Daresbury, Warrington WA4 4AD, United Kingdom

J. F. Sharpey-Schafer
iThemba Laboratory for Accelerator Based Sciences, P.O. Box 722, Somerset West 7129, Republic of South Africa
(Received 15 August 2002; published 31 December 2002)

The reactions ^{152}Sm$(\alpha,3n)$ at 37 MeV and ^{124}Sn$(^{36}$S$,\alpha 3n)$ at 165 MeV were used to produce high-spin states in the transitional rare-earth nucleus ^{153}Gd. Significant extensions in angular momentum and excitation energy with respect to earlier work were achieved and several new rotational sequences were observed. The rotational behavior of ^{153}Gd is described in terms of quasiparticle assignments and the observed alignment properties are analyzed within the framework of the cranked shell model. Detailed comparisons with other $N=89$ nuclei are presented. These have led to corrections to the ^{157}Er level scheme.

DOI: 10.1103/PhysRevC.66.064320 PACS number(s): 21.10.Re, 23.20.Lv, 27.70.+q

I. INTRODUCTION

It has been long recognized [1] that for the nuclei in the rare-earth transitional region, a sudden change occurs from vibrational behavior ($N \leqslant 88$) to rotational behavior ($N \geqslant 90$). Furthermore, this change is most dramatic in the Gd isotopes. Thus, ^{153}Gd lies at the heart of this region where ground-state deformation grows rapidly with increasing neutron number. A primary motivation for this study was to investigate to what degree the $N=89$ isotones ^{151}Sm, ^{153}Gd, ^{155}Dy, and ^{157}Er remain similar in behavior at high spin, and to search for and focus on any characteristics that are different. In effect, a systematic look at these nuclei becomes a study of the changing proton Fermi level and of the stability of these nuclei against this change.

The Sm and Gd isotopes have not been studied to as high a spin as their heavier neighbors Dy, Er, and Yb [2–8] because no suitable stable target/heavy-ion beam combinations are available to populate them via the dominant xn decay channels in fusion-evaporation reactions. However, with a powerful detector array such as Gammasphere [9], we have obtained high-spin information from a $(HI,\alpha xn)$ reaction even though it may account for $< 1\%$ of the total cross section. To fully exploit the latter, it was necessary to perform an experiment to clarify the low-spin region of ^{153}Gd. Therefore, a second experiment was carried out using the Florida State University (FSU) Pitt array [10] with the (α,xn) reaction.

II. EXPERIMENTAL TECHNIQUES

A. Low-spin study

The experiment to study the low-spin structure of ^{153}Gd was carried out at the FN tandem-superconducting linear accelerator facility at Florida State University. The ^{152}Sm$(\alpha,3n)$ reaction was employed with a beam energy of 37 MeV. The target consisted of a 1-mg/cm^2 foil of enriched ^{152}Sm. Emitted γ rays were collected using nine Compton-suppressed Hewlett Packard (HP) Ge detectors of the FSU-Pitt array [10]. The Compton-suppressed spectrometers were placed at angles of 35°(2), 90°(3), and 145°(4) to the beam direction, where the numbers in parentheses indicate the number of detectors at that particular angle. A total of 90×10^6 events were recorded when two or more suppressed

*Present address: Savannah River Technology Center, Westinghouse Savannah River Company, Aiken, SC 29802.
†Present address: Department of Physics, United States Naval Academy, Annapolis, MD 21402.
‡Present address: Argonne National Laboratory, Argonne, IL 60439.
§Present address: CRT Holdings Inc, 11030 Cochiti SE, Albuquerque, NM 87123.
‖Present address: Department of Physics, DePaul University, Chicago, IL 60614-3504.
¶Present address: Bio-Imaging Research, Inc., Lincolnshire, IL 60069.

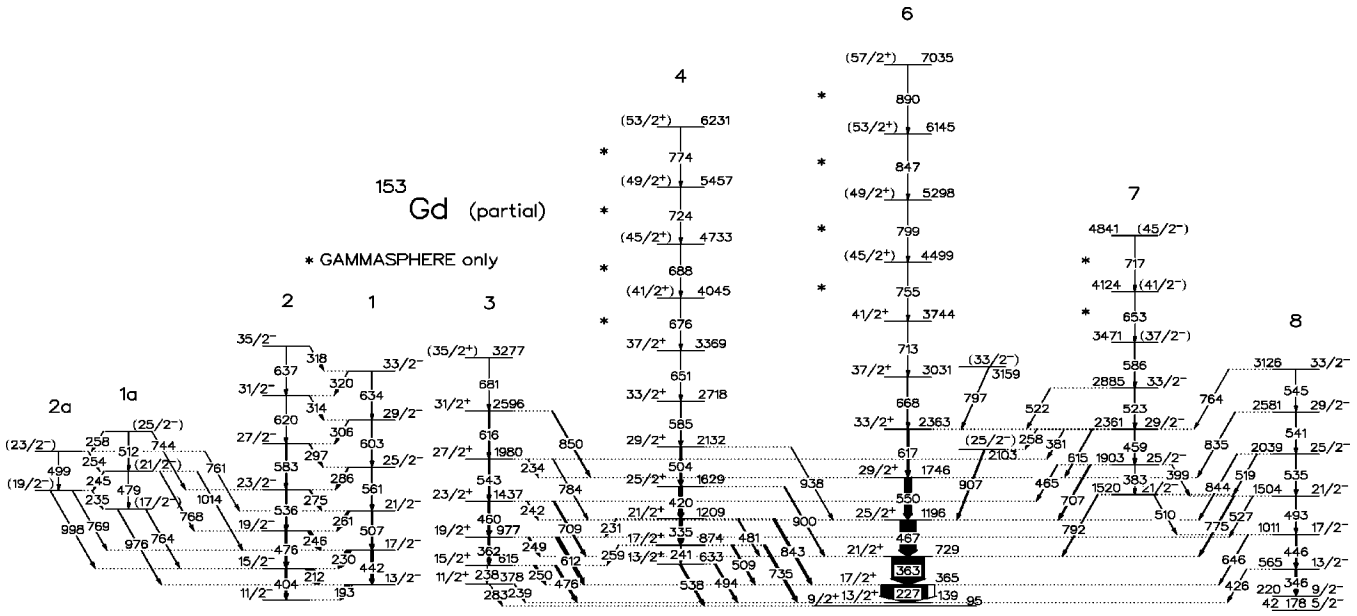

FIG. 1. Partial level scheme of ^{153}Gd (part a) from the α-induced reaction except for the transitions labeled by an asterisk which are extensions from the ^{36}S reaction. Brackets indicate tentative spin and parity assignments.

Ge detector signals were detected within a 100-ns coincidence window. Events corresponding to the $3n$, ^{153}Gd channel accounted for approximately 90% of the reaction cross section. The level scheme analysis was performed using the program ESCL8R [11,12] To aid in the assignment of spins to the states in the level scheme, γ-ray angular correlations were measured. These correlation measurements were made by constructing a two-dimensional matrix with events from the three detectors positioned at 90° on one axis, and coincident events from the six detectors positioned at 35° and 145° on the other. Within these matrices, gates were set on uncontaminated stretched $E2$ transitions from both axes and the observed intensity of the peaks in the corresponding projections were used to calculate the ratio $I(90°,35°)/I(35°,90°)$. Ratios of ≈ 1 for stretched $E2$ transitions and ≈ 0.5 for dipole transitions were found. (For the strongly coupled sequences [bands 1, 2, 1(a), 2(a)], gates were placed on $\Delta I=1$ transitions (see below) which resulted in ratios of ≈ 2.5 for stretched $E2$ transitions and ≈ 1.0 for dipole transitions.)

B. High-spin study

The ^{124}Sn+ ^{36}S reaction at a beam energy of 165 MeV was employed to populate high-spin states chiefly in Dy isotopes via the xn channels at the Lawrence Berkeley National Laboratory's 88 Inch Cyclotron facility. The target consisted of two stacked 400-μg/cm^2 enriched ^{124}Sn foils. Emitted γ rays were collected using 93 HP Ge detectors of the Gammasphere array [9]. Approximately 1.26×10^9 events were recorded where at least five suppressed detectors fired within the coincidence window ($\approx$500 ns). Events corresponding to the $\alpha 3n$ channel populating ^{153}Gd accounted for $<1\%$ of the total data collected. A coincidence data analysis was performed using the program LEVIT8R [11]. Only states in bands 4, 6, and 7 (see below) were observed in these data. The new transitions added to the ^{153}Gd level scheme were assumed to be of $E2$ character for reasons outlined below.

III. EXPERIMENTAL RESULTS

Previously, high-spin states in ^{153}Gd have been studied by Rezanka *et al.* [13], Lövhöiden *et al.* [14], and Rekstad *et al.* [15]. Our results confirm the majority of the previous assignments. The deduced level scheme from the present work is shown in Figs. 1 and 2. The levels are grouped in sequences having the same parity π and signature α connected by stretched $E2$ transitions. The ordering of transitions was determined from coincidence relationships and intensity arguments. Excitation energies (relative to the $3/2^-$ ground-state level), γ-ray energies, γ-ray transition intensities, DCO ratios, and spin-parity assignments from the α induced reaction can be found in Table I. Transition energies assigned to ^{153}Gd from the Gammasphere experiment are shown in the level scheme only.

A. Positive-parity states

1. The band based on the 138.8-keV $13/2^+$ *level(band 6)*

Band 6 is the lowest-energy positive-parity band and remains the yrast band over the entire spin region observed in both experiments. Previously observed to spin $33/2^+$ [14], it has been extended to $41/2^+$ in the α experiment and to $57/2^+$ in the ^{36}S-induced reaction. A triple coincidence spectrum from the ^{36}S Gammasphere experiment gated by the 668- and 713-keV transitions is shown in Fig. 3(a). The spectrum of transitions in coincidence with the 668-keV $37/2^+ \rightarrow 33/2^+$ transition is shown in Fig. 3(b). The $9/2^+$ state is the lowest spin state observed in this band at an excitation energy of 95.1-keV. Early transfer studies [16,17] had placed the $13/2^+$ level in this band at 139 ± 2 keV. This level was

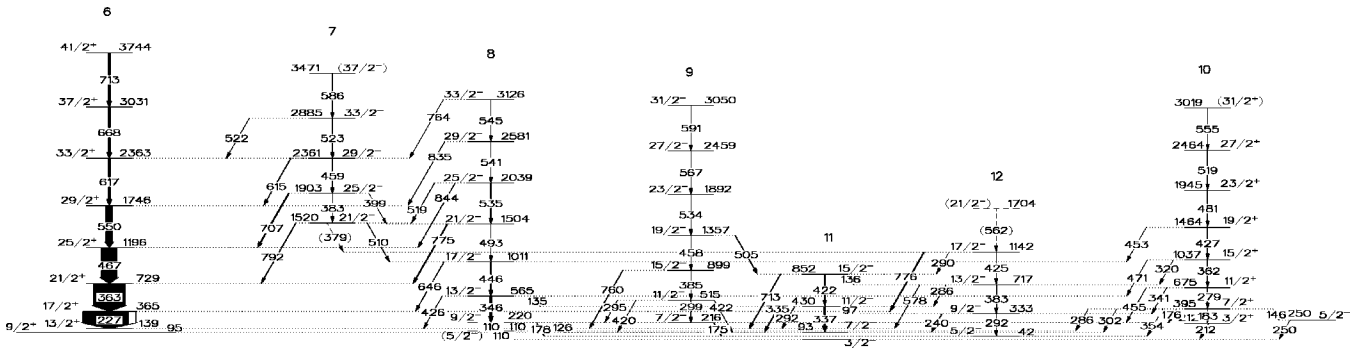

FIG. 2. Partial level scheme of ^{153}Gd (part b) from the α-induced reaction. Brackets indicate tentative spin and parity assignments.

assigned as 134.7 keV [14] based on tentative γ-ray assignments later shown to be incorrect [15]. The current work (see Fig. 1) firmly determines that the $13/2^+$ level is placed at 138.8 keV. The most convincing evidence for this assignment is the previously unseen electric dipole decays from levels in band 8 to levels in band 6, see below. As seen in Fig. 3(a) the highest transitions (755–890 keV) form a natural extension to this band structure, and an $E2$ character is thus justified.

2. The band based on the 615.3-keV 15/2$^+$ level (band 3)

The states of 15/2 and 19/2 were identified by Rekstad *et al.* [15] in disagreement with previous assignments [14]. Our assignments confirm the in band coincidence relationships of Rekstad *et al.* and extend this band from $19/2^+$ to $35/2^+$ (but they add 4.1 keV to the level energies of the previously seen 15/2 and 19/2 levels).

3. The band based on the 632.8-keV-13/2$^+$ level (band 4)

Band 4 is a new sequence observed up to a spin of $37/2^+$ in the α-induced experiment and extended up to $53/2^+$ in the ^{36}S experiment [Fig. 4(a)]. A spectrum of the transitions in coincidence with the 650.9-keV $37/2^+ \rightarrow 33/2^+$ transition (α experiment) is shown in Fig. 4(b). The spin and parity assignments for this band are based on the following arguments. The transitions connecting the level at 632.8 keV to the levels at 95.1 and 138.8 keV in band 6 have a ratio R_{DCO} of 1.1 ± 0.1 and 1.0 ± 0.1, respectively. These transitions restrict the possible spins of this level to 9/2, 11/2, and 13/2. However, intensity considerations strongly favor the 13/2 assignment.The eight transitions connecting band 4 to band 6 are then of $I \rightarrow I-2$ and $I \rightarrow I$ character, consistent with measured R_{DCO} values of ~ 1. The positive-parity assignment will be discussed further in Sec. IV. The argument given above for the highest transitions in band 6 also applies to the $E2$ asignment for the 676–774 keV lines.

4. The band based on the 212.1-keV 3/2$^+$ level (band 10)

The bandhead level at 212.1 keV has been identified in transfer data [16,17] and assigned spin and parity $I^\pi = 3/2^+$. Our DCO analysis of the many transitions exiting this band are consistent with this assignment (see Table I). Band 10 had been previously observed tentatively to $15/2^+$ [15]. With the present data we have now traced this band up to a spin of 31/2.

B. Negative-parity states

1. The bands based on the 171.4-keV 11/2$^-$ level (bands 1 and 1a and 2 and 2a)

Bands 1 and 2 are strongly coupled sequences built on the $I^\pi = 11/2^-$, 79-μs isomer. They were previously observed to $27/2^-$ [14]. Our results confirm these measurements and extend the band spin to $35/2^-$. Transitions in coincidence with the $13/2^- \rightarrow 11/2^-$ 192.5- keV γ ray can be seen in Fig. 5. Bands 1a and 2a are observed for the first time in the present work, and are connected to levels in both bands 1 and 2. The lowest-energy level at 1340 keV, decays via the 975.8-keV ($R_{DCO} = 3.0\pm0.6$) transition to the $13/2^-$ level in band 1 and via the 764.3-keV ($R_{DCO} = 0.8\pm0.2$) transition to the $15/2^-$ level in band 2. The R_{DCO} values of these transitions, determined from gates on the 192.5-keV ($\Delta I = 1$) transition, suggest a spin assignment of $17/2^-$. The nonobservation of transitions to the $11/2^-$ level rule out lower-spin, negative-parity assignments. The R_{DCO} values of the linking transitions rule out $15/2^+$. In band transitions of both $\Delta I = 1$ and $\Delta I = 2$ character fix the spins of the remaining states in both bands 1a and 2a.

2. The band based on the 1520.2-keV 21/2$^-$ level (band 7)

The spin and parity of the level at 1520.2 keV can be firmly established as $21/2^-$ with the stretched $E2$ transitions 509.6 and 519.2 keV connecting this level to the $17/2^-$ and $25/2^-$ levels of band 8. An R_{DCO} value of 1.0 ± 0.1 for the 791.5-keV transition connecting the 1520.2-keV level to the 728.6-keV level in band 6 is consistent with that of a transition with an unstretched $E1$ character.

3. The bands based on the 110-keV 5/2$^-$ level (bands 8,9)

Band 8 has been established by Rekstad *et al.* [15] via the decays of a 126.5-keV transition to the 93.3-keV $7/2^-$ level and a 178-keV transition to the $5/2^-$, 41.5-keV level. A measured ratio $R_{DCO} = 0.5\pm0.1$ for the 126.5-keV and $R_{DCO} = 1.1\pm0.2$ for the 178-keV transitions decaying from the $9/2^-$ level to levels of $7/2^-$ and $5/2^-$, respectively, are consistent with previous assignments. An additional weak decay branch from the $9/2^-$ 219.7-keV level is observed through the 110-keV $5/2^-$ level with the self-coincidence of the 110-keV doublet. The spin and parity of the 216.3-keV level of band 9 were assigned as $7/2^-$ from beta decay studies [19],

TABLE I. Data for ^{153}Gd from the α-induced reaction.

E_x (keV)	E_γ (keV) [a]	I_γ^{rel} [b]	DCO ratio [c]	Multi. [d]	I_i^π	I_f^π	Band$_f$
Band 1							
363.8	192.5	27 ± 3	0.9±0.1 [c]	$M1/E2$	$\frac{13}{2}^-$	$\frac{11}{2}^-$	2
805.4	229.8	16.1± 1	0.9±0.1 [c]	$M1/E2$	$\frac{17}{2}^-$	$\frac{15}{2}^-$	2
	441.5	8.7± 0.5	2.9±0.2 [c]	$E2$	$\frac{17}{2}^-$	$\frac{13}{2}^-$	
1312.7	261.2	6.5± 0.4	1.0±0.1 [c]	$M1/E2$	$\frac{21}{2}^-$	$\frac{19}{2}^-$	2
	507.4	7.3± 0.4	2.8±0.2 [c]	$E2$	$\frac{21}{2}^-$	$\frac{17}{2}^-$	
1873.6	286.4	2.4± 0.2	1.0±0.1 [c]	$M1/E2$	$\frac{25}{2}^-$	$\frac{23}{2}^-$	2
	560.9	4.1± 0.3	3.1±0.2 [c]	$E2$	$\frac{25}{2}^-$	$\frac{21}{2}^-$	
2476.4	306.0	0.8± 0.2	0.8±0.2 [c]	$M1/E2$	$\frac{29}{2}^-$	$\frac{27}{2}^-$	2
	602.8	2.6± 0.2	2.3±0.2 [c]	$E2$	$\frac{29}{2}^-$	$\frac{25}{2}^-$	
3109.9	319.5	<0.5		$M1/E2$	$\frac{33}{2}^-$	$\frac{31}{2}^-$	2
	633.5	0.7± 0.2		$E2$	$\frac{33}{2}^-$	$\frac{29}{2}^-$	
Band 2							
575.6	211.8	24.3± 1.5	1.0±0.1 [c]	$M1/E2$	$\frac{15}{2}^-$	$\frac{13}{2}^-$	1
	404.2	5.9± 0.4	2.2±0.2 [c]	$E2$	$\frac{15}{2}^-$	$\frac{11}{2}^-$	
1051.6	246.3	10.5± 0.6	0.9±0.1 [c]	$M1/E2$	$\frac{19}{2}^-$	$\frac{17}{2}^-$	1
	476.0	8.0± 0.5	2.9±0.2 [c]	$E2$	$\frac{19}{2}^-$	$\frac{15}{2}^-$	
1587.3	274.5	3.9± 0.2	1.0±0.1 [c]	$M1/E2$	$\frac{23}{2}^-$	$\frac{21}{2}^-$	1
	535.6	5.6± 0.3	2.9±0.2 [c]	$E2$	$\frac{23}{2}^-$	$\frac{19}{2}^-$	
2170.5	296.9	1.3±0.1	0.9±0.2 [c]	$M1/E2$	$\frac{27}{2}^-$	$\frac{25}{2}^-$	1
	583.2	3.1±0.2	3.2±0.3 [c]	$E2$	$\frac{27}{2}^-$	$\frac{23}{2}^-$	
2790.3	313.8	0.4±0.1		$M1/E2$	$\frac{31}{2}^-$	$\frac{29}{2}^-$	1
	619.7	1.4±0.1	3.2±0.4 [c]	$E2$	$\frac{31}{2}^-$	$\frac{27}{2}^-$	
3427.5	317.6	<0.5		$M1/E2$	$\frac{35}{2}^-$	$\frac{33}{2}^-$	1
	637.3	0.4 ±0.1		$E2$	$\frac{35}{2}^-$	$\frac{31}{2}^-$	
Band 1a							
1340	764.3	1.0 ±0.1	0.8±0.2 [c]	$(M1/E2)$	$(\frac{17}{2}^-)$	$\frac{15}{2}^-$	2
	975.8	1.5 ±0.1	3.0±0.6 [c]	$(E2)$	$(\frac{17}{2}^-)$	$\frac{13}{2}^-$	1
1819	245	0.7 ±0.1		$M1/E2$	$(\frac{21}{2}^-)$	$(\frac{19}{2}^-)$	2a
	479	<0.5		$E2$	$(\frac{21}{2}^-)$	$(\frac{17}{2}^-)$	
	767.8	0.6 ±0.1	0.7±0.2 [c]	$(M1/E2)$	$(\frac{21}{2}^-)$	$\frac{19}{2}^-$	2
	1014	0.8 ±0.1	2.1±0.2 [c]	$(E2)$	$(\frac{21}{2}^-)$	$\frac{17}{2}^-$	1
2331	257	0.6 ±0.1		$M1/E2$	$(\frac{25}{2}^-)$	$(\frac{23}{2}^-)$	2a
	512	<0.5		$E2$	$(\frac{25}{2}^-)$	$(\frac{21}{2}^-)$	
	744	<0.5		$(M1/E2)$	$(\frac{25}{2}^-)$	$\frac{23}{2}^-$	2
Band 2a							
1574	234.6	0.6 ±0.1		$M1/E2$	$(\frac{19}{2}^-)$	$(\frac{17}{2}^-)$	1a
	769.1	0.8 ±0.1		$(M1/E2)$	$(\frac{19}{2}^-)$	$\frac{17}{2}^-$	1
	998.4	0.8 ±0.1	2.2±0.5 [c]	$(E2)$	$(\frac{19}{2}^-)$	$\frac{15}{2}^-$	2
2073	254	0.6 ±0.1		$M1/E2$	$(\frac{23}{2}^-)$	$(\frac{21}{2}^-)$	1a
	499	<0.5		$E2$	$(\frac{23}{2}^-)$	$(\frac{19}{2}^-)$	
	761	<0.5		$(M1/E2)$	$(\frac{23}{2}^-)$	$\frac{21}{2}^-$	1
Band 3							
(378)	239	0.6 ±0.1		$(M1/E2)$	$(\frac{11}{2}^+)$	$\frac{13}{2}^+$	6
	283	<0.5		$(M1/E2)$	$(\frac{11}{2}^+)$	$\frac{9}{2}^+$	6
615.3	238	0.9 ±0.1		$(E2)$	$\frac{15}{2}^+$	$(\frac{11}{2}^+)$	
	249.9 [e]	7.5 ±0.5	0.8±0.2	$M1/E2$	$\frac{15}{2}^+$	$\frac{17}{2}^+$	6
	476.4	7.4 ±0.6	1.1±0.1	$M1/E2$	$\frac{15}{2}^+$	$\frac{13}{2}^+$	6

TABLE I. (*Continued*).

E_x (keV)	E_γ (keV) [a]	I_γ^{rel} [b]	DCO ratio [c]	Multi. [d]	I_i^π	I_f^π	Band$_f$
977.3	248.8 [e]	5.4 ±0.4	0.8±0.2	$M1/E2$	$\frac{19}{2}^+$	$\frac{21}{2}^+$	6
	361.9 [e]	6.4 ±0.4		$E2$	$\frac{19}{2}^+$	$\frac{15}{2}^+$	
	611.9	12.7 ±0.8	1.4±0.2	$M1/E2$	$\frac{19}{2}^+$	$\frac{17}{2}^+$	6
1437.3	241.7	1.7 ±0.1	0.6±0.2	$M1/E2$	$\frac{23}{2}^+$	$\frac{25}{2}^+$	6
	460.0	8.1 ±0.5	1.1±0.1	$E2$	$\frac{23}{2}^+$	$\frac{19}{2}^+$	
	708.7	5.5 ±0.4	1.3±0.2	$M1/E2$	$\frac{23}{2}^+$	$\frac{21}{2}^+$	6
1980.1	234.1	0.6 ±0.1	0.5±0.2	$M1/E2$	$\frac{27}{2}^+$	$\frac{29}{2}^+$	6
	543.1	5.6 ±0.3	1.0±0.1	$E2$	$\frac{27}{2}^+$	$\frac{23}{2}^+$	
	784.5	1.3 ±0.1	1.2±0.2	$M1/E2$	$\frac{27}{2}^+$	$\frac{25}{2}^+$	6
2596.1	616.3	2.3 ±0.2	1.0±0.2	$E2$	$\frac{31}{2}^+$	$\frac{27}{2}^+$	
	849.7	4.8 ±0.2	0.5±0.1	$M1/E2$	$\frac{31}{2}^+$	$\frac{29}{2}^+$	6
3276.6	680.5	<0.5		$E2$	$(\frac{35}{2}^+)$	$\frac{31}{2}^+$	
Band 4							
632.8	493.9	5.4 ±0.4	1.1±0.1	$M1/E2$	$\frac{13}{2}^+$	$\frac{13}{2}^+$	6
	537.6	6.6 ±0.5	1.0±0.1	$E2$	$\frac{13}{2}^+$	$\frac{9}{2}^+$	6
874.0	241.1	3.0 ±0.2	1.1±0.1	$E2$	$\frac{17}{2}^+$	$\frac{13}{2}^+$	
	258.7	0.9 ±0.1	0.3±0.1	$M1/E2$	$\frac{17}{2}^+$	$\frac{15}{2}^+$	3
	508.8	5.8 ±0.4	1.1±0.1	$M1/E2$	$\frac{17}{2}^+$	$\frac{17}{2}^+$	6
	734.9	8.6 ±0.6	1.0±0.1	$E2$	$\frac{17}{2}^+$	$\frac{13}{2}^+$	6
1208.9	231.2	0.9 ±0.1	≪1	$M1/E2$	$\frac{17}{2}^+$	$\frac{15}{2}^+$	3
	335.0	13.4 ±0.8	1.0±0.1	$E2$	$\frac{21}{2}^+$	$\frac{17}{2}^+$	
	480.5	3.0 ±0.2	0.9±0.1	$M1/E2$	$\frac{21}{2}^+$	$\frac{21}{2}^+$	6
	843.3	8.4 ±0.5	0.9±0.1	$E2$	$\frac{21}{2}^+$	$\frac{17}{2}^+$	6
1628.8	420.0	15.2 ±0.9	1.1±0.1	$E2$	$\frac{25}{2}^+$	$\frac{21}{2}^+$	
	900.0	3.0 ±0.2	0.9±0.1	$E2$	$\frac{25}{2}^+$	$\frac{21}{2}^+$	6
2132.4	503.5	9.2 ±0.6	1.0±0.1	$E2$	$\frac{29}{2}^+$	$\frac{25}{2}^+$	
	937	0.5 ±0.1		$E2$	$\frac{29}{2}^+$	$\frac{25}{2}^+$	6
2717.6	585.2	3.9 ±0.3	1.0±0.1	$E2$	$\frac{33}{2}^+$	$\frac{29}{2}^+$	
3368.5	650.9	1.1 ±0.1	0.9±0.2	$E2$	$\frac{37}{2}^+$	$\frac{33}{2}^+$	
4044.8	676.3	<0.5		$(E2)$	$(\frac{41}{2}^+)$	$\frac{37}{2}^+$	
Band 6							
365.3	226.5	—	1.1±0.1	$E2$	$\frac{17}{2}^+$	$\frac{13}{2}^+$	
728.5	363.2 [e]	≡133	1.0±0.1	$E2$	$\frac{21}{2}^+$	$\frac{17}{2}^+$	
1195.7	467.2	67 ± 8	1.0±0.1	$E2$	$\frac{25}{2}^+$	$\frac{21}{2}^+$	
1746.2	550.3	28.4 ±1.7	1.0±0.1	$E2$	$\frac{29}{2}^+$	$\frac{25}{2}^+$	
2362.8	616.6	10.0 ±0.6	1.0±0.1	$E2$	$\frac{33}{2}^+$	$\frac{29}{2}^+$	
3031.2	668.4	2.1 ±0.2	1.0±0.1	$E2$	$\frac{37}{2}^+$	$\frac{33}{2}^+$	
3743.9	712.6	0.4 ±0.1	0.8±0.2	$E2$	$\frac{41}{2}^+$	$\frac{37}{2}^+$	
Band 7							
1520.2	(379)			$(E2)$	$\frac{21}{2}^-$	$\frac{17}{2}^-$	12
	509.6	1.3± 0.1	1.0±0.1	$E2$	$\frac{21}{2}^-$	$\frac{17}{2}^-$	8
	791.5	2.5± 0.2	1.0±0.1	$E1$	$\frac{21}{2}^-$	$\frac{21}{2}^+$	6
1902.7	382.7	<0.5		$E2$	$\frac{25}{2}^-$	$\frac{21}{2}^-$	
	398.9	<0.5	1.5±0.4	$E2$	$\frac{25}{2}^-$	$\frac{21}{2}^-$	8
	465.2	1.6± 0.2		$E1$	$\frac{25}{2}^-$	$\frac{23}{2}^+$	3
	707.1	4.5± 0.3	1.1±0.1	$E1$	$\frac{25}{2}^-$	$\frac{25}{2}^+$	6
2361.2	381.2	0.6± 0.1		$E1$	$\frac{29}{2}^-$	$\frac{27}{2}^+$	3
	458.5	2.1± 0.2	1.2±0.2	$E2$	$\frac{29}{2}^-$	$\frac{25}{2}^-$	
	614.8	2.2± 0.2		$E1$	$\frac{29}{2}^-$	$\frac{29}{2}^+$	6
	258.1	<0.5		$(M1)$	$\frac{29}{2}^-$	$(\frac{27}{2}^-)$	2103.3
2884.7	522.4	0.7± 0.2	1.0±0.2	$E1$	$\frac{33}{2}^-$	$\frac{33}{2}^+$	6

TABLE I. (*Continued*).

E_x (keV)	E_γ (keV) [a]	I_γ^{rel} [b]	DCO ratio [c]	Multi. [d]	I_i^π	I_f^π	Band$_f$
	523.2	1.9± 0.2	1.0±0.1	$E2$	$\frac{33}{2}^-$	$\frac{29}{2}^-$	
3471.0	586.3	0.7± 0.1	1.3±0.2	$(E2)$	$(\frac{37}{2}^-)$	$\frac{33}{2}^-$	
Band 8							
219.7	110	<0.5		$(E2)$	$\frac{9}{2}^-$	$\frac{5}{2}^-$	109.8
	126.5	4.6 ±1.3	0.5±0.1	$M1/E2$	$\frac{9}{2}^-$	$\frac{7}{2}^-$	93.3
	178.2	1.4 ±0.4	1.1±0.2	$E2$	$\frac{9}{2}^-$	$\frac{5}{2}^-$	
565.2	135	<0.5	0.5±0.2	$M1/E2$	$\frac{13}{2}^-$	$\frac{11}{2}^-$	9
	345.5	7.4 ±0.5	1.0±0.1	$E2$	$\frac{13}{2}^-$	$\frac{9}{2}^-$	
	426.1	0.6 ±0.1	1.3±0.2	$E1$	$\frac{13}{2}^-$	$\frac{13}{2}^+$	6
1010.8	445.7	5.5 ±0.4	1.0±0.1	$E2$	$\frac{17}{2}^-$	$\frac{13}{2}^-$	
	645.7	1.5 ±0.2		$E1$	$\frac{17}{2}^-$	$\frac{17}{2}^+$	6
1504.1	493.4	1.5 ±0.1	0.9±0.1	$E2$	$\frac{21}{2}^-$	$\frac{17}{2}^-$	
	526.8	0.8 ±0.1	0.4±0.2	$E1$	$\frac{21}{2}^-$	$\frac{19}{2}^+$	3
	775.3	3.8 ±0.3	1.0±0.1	$E1$	$\frac{21}{2}^-$	$\frac{21}{2}^+$	6
2039.4	519.2	1.1 ±0.1	1.3±0.2	$E2$	$\frac{25}{2}^-$	$\frac{21}{2}^-$	7
	535.3	2.5 ±0.2	0.9±0.2	$E2$	$\frac{25}{2}^-$	$\frac{21}{2}^-$	
	843.7	1.6 ±0.1	0.8±0.2	$E1$	$\frac{25}{2}^-$	$\frac{25}{2}^+$	6
2580.9	541.4	1.6 ±0.2	1.0±0.1	$E2$	$\frac{29}{2}^-$	$\frac{25}{2}^-$	
	834.8	0.9 ±0.1	0.9±0.2	$E1$	$\frac{29}{2}^-$	$\frac{29}{2}^+$	6
3126.4	545.4	0.6 ±0.1		$(E2)$	$(\frac{33}{2}^-)$	$\frac{29}{2}^-$	
	763.7	<0.5		$(E1)$	$(\frac{33}{2}^-)$	$\frac{33}{2}^+$	6
Band 9							
430.1	97	0.4 ±0.1		$M1/E2$	$\frac{11}{2}^-$	$\frac{9}{2}^-$	12
	291.7	1.1 ±0.2		$E1$	$\frac{11}{2}^-$	$\frac{13}{2}^+$	6
	335	3 ±1		$E1$	$\frac{11}{2}^-$	$\frac{9}{2}^+$	6
	337	7.8 ±0.9	1.3±0.2	$E2$	$\frac{11}{2}^-$	$\frac{7}{2}^-$	
852.2	422.1	2.9 ±0.2	1.0±0.1	$E2$	$\frac{15}{2}^-$	$\frac{11}{2}^-$	
	713.2	2.7 ±0.3	0.6±0.1	$E1$	$\frac{15}{2}^-$	$\frac{13}{2}^+$	6
1357.2	458.3	0.8 ±0.1	0.9±0.1	$E2$	$\frac{19}{2}^-$	$\frac{15}{2}^-$	11
	505.2	2.3 ±0.2	1.1±0.1	$E2$	$\frac{19}{2}^-$	$\frac{15}{2}^-$	
1892	534.3	1.3 ±0.1	1.2±0.2	$E2$	$\frac{23}{2}^-$	$\frac{19}{2}^-$	
2459	567.3	0.7 ±0.1	0.9±0.1	$E2$	$\frac{27}{2}^-$	$\frac{23}{2}^-$	
3050	591	<0.5		$E2$	$(\frac{31}{2}^-)$	$\frac{27}{2}^-$	
Band 10							
212.1	212.1	1.0 ±0.5	0.6±0.1	$E1$	$(\frac{3}{2}^+)$	$\frac{3}{2}^-$	(0)
395.5	146.0	<0.5	0.5±0.2	$E1$	$\frac{7}{2}^+$	$\frac{5}{2}^-$	249.6
	176	<0.5	≪1	$E1$	$\frac{7}{2}^+$	$\frac{9}{2}^-$	8
	183.4	<0.5	0.9±0.1	$E2$	$\frac{7}{2}^+$	$(\frac{3}{2}^+)$	
	285.6	0.6 ±0.1	0.6±0.1	$E1$	$\frac{7}{2}^+$	$\frac{5}{2}^-$	109.8
	302.0	0.4 ±0.1	1.1±0.2	$E1$	$\frac{7}{2}^+$	$\frac{7}{2}^-$	93.3
	353.9	0.4 ±0.1	0.6±0.1	$E1$	$\frac{7}{2}^+$	$\frac{5}{2}^-$	8
674.8	279.4	1.8 ±0.1	1.0±0.1	$E2$	$\frac{11}{2}^+$	$\frac{7}{2}^+$	
	341.5	0.7 ±0.1	0.8±0.2	$E1$	$\frac{11}{2}^+$	$\frac{9}{2}^-$	12
	455	0.6 ±0.2		$E1$	$\frac{11}{2}^+$	$\frac{9}{2}^-$	8
1036.6	320	<0.5		$E1$	$\frac{15}{2}^+$	$(\frac{13}{2}^-)$	10
	361.8	2.0 ±0.2	1.1±0.1	$E2$	$\frac{15}{2}^+$	$\frac{11}{2}^+$	
	471	0.5 ±0.1		$E1$	$\frac{15}{2}^+$	$\frac{13}{2}^-$	8
1464.0	427.4	2.2 ±0.2	1.1±0.1	$E2$	$\frac{19}{2}^+$	$\frac{15}{2}^+$	
	453.1	0.3 ±0.1	0.6±0.1	$E1$	$\frac{19}{2}^+$	$\frac{17}{2}^-$	8
1945	481.1	1.2 ±0.1	1.2±0.3	$E2$	$\frac{23}{2}^+$	$\frac{19}{2}^+$	

TABLE I. (*Continued*).

E_x (keV)	E_γ (keV) [a]	I_γ^{rel} [b]	DCO ratio [c]	Multi. [d]	I_i^π	I_f^π	Band$_f$
2464	519.2	0.6 ±0.1	0.9±0.2	$E2$	$\frac{27}{2}^+$	$\frac{23}{2}^+$	
3019	555	<0.5		$E2$	$(\frac{31}{2}^+)$	$\frac{27}{2}^+$	
Band 11							
216.3	174.8	≃2	0.6±0.2	$M1/E2$	$\frac{7}{2}^-$	$\frac{5}{2}^-$	41.5
514.9	295.3	0.6 ±0.1	≪1	$M1/E2$	$\frac{11}{2}^-$	$\frac{9}{2}^-$	
	298.6	1.5 ±0.2	1.1±0.2	$E2$	$\frac{11}{2}^-$	$\frac{7}{2}^-$	93.3
	419.6	0.6 ±0.1		$E1$	$\frac{11}{2}^-$	$\frac{9}{2}^+$	6
	422.0	0.6 ±0.1		$E2$	$\frac{11}{2}^-$	$\frac{7}{2}^-$	9
899.2	384.5	0.6 ±0.1	1.2±0.3	$E2$	$\frac{15}{2}^-$	$\frac{11}{2}^-$	
	760.2	2.1 ±0.5	1.2±0.3	$E1$	$\frac{15}{2}^-$	$\frac{13}{2}^+$	
Band 12							
333.3	240.1	2.0 ±0.3	0.4±0.1	$M1/E2$	$\frac{9}{2}^-$	$\frac{7}{2}^-$	93.3
	291.9	1.7 ±0.2	1.0±0.1	$E2$	$\frac{9}{2}^-$	$\frac{5}{2}^-$	41.5
716.6	286.5	0.7 ±0.1	0.4±0.2	$M1/E2$	$\frac{13}{2}^-$	$\frac{11}{2}^-$	9
	383.3	2.0 ±0.2	1.0±0.1	$E2$	$\frac{13}{2}^-$	$\frac{9}{2}^-$	
	577.8	0.9 ±0.2		$E1$	$\frac{13}{2}^-$	$\frac{13}{2}^+$	6
1141.5	289.6	<0.5		$M1/E2$	$\frac{17}{2}^-$	$\frac{15}{2}^-$	9
	424.9	0.9 ±0.1	1.2±0.2	$E2$	$\frac{17}{2}^-$	$\frac{13}{2}^-$	
	(776)	3.7 ±0.1		$E1$	$\frac{17}{2}^-$	$\frac{17}{2}^+$	6
(1704)	(562)	0.5 ±0.1		$(E2)$	$(\frac{21}{2}^-)$	$\frac{17}{2}^-$	
Other levels							
110	110		0.5±0.1	$M1/E2$	$\frac{5}{2}^-$	$\frac{3}{2}^-$	0.0
249.6	249.6	0.3 ±0.1		$M1/E2$	$\frac{5}{2}^-$	$\frac{3}{2}^-$	0.0
2103.3	907.5	4.3 ±0.3	0.5±0.1	$(E1)$	$(\frac{27}{2}^-)$	$\frac{25}{2}^+$	6

[a]Accurate to 0.2 keV for most transitions. For weak or contaminated transitions, accurate to 0.5 keV or 1 keV.
[b]Relative gamma-ray intensities [I_γ (363.0 of band 6)≡133].
[c]Angular correlation ratio $I(90°,35°)/I(35°,90°)$, where $I(90°,35°)$ [or $I(35°,90°)$] is the intensity measured by the detectors at 35° (or 90°) which are in coincidence with the 90° (or 35°) detectors. Ratios for bands 1, 1a, 2, and 2a are determined from gates on $\Delta I=1$ transitions.
[d]Deduced gamma-ray multipolarity.
[e]Unresolved gamma-ray doublet in the angular correlation spectra. Angular correlation ratio given for sum of unresolved transitions quoted.

consistent with a measured ratio $R_{DCO}=0.6\pm0.2$ for the 174.8-keV transition populating the 41.5-keV, $5/2^-$ level. The $11/2^-$ and $15/2^-$ levels at 514.8, and 898.7 keV have been established by Rekstad *et al.* [15]. While we agree on the location of these levels (514.9 and 899.2 keV), we find no evidence for a ~334-keV γ ray linking the 898.7-keV, $15/2^-$ level to the 565.2-keV, $13/2^-$ level of band 8. A 419.4-keV γ ray was assigned [15] as the $19/2^-\rightarrow15/2^-$ transition based on a coincidence with the 384.4-keV $15/2^-\rightarrow11/2^-$ transition, however, it decays from the $11/2^-$ level and does not populate the $15/2^-$ level. The $19/2^-$ level is now located at 1357.2 keV and decays via the 505.2- and 458.3-keV $E2$ transitions to $15/2^-$ levels in both bands 9 and 11, respectively.

4. The bands based on the 3/2⁻ ground-state level (bands 11,12)

The $3/2^-$, $5/2^-$, and $7/2^-$ levels are known members of this ground-state band. Two new states have been added to band 11 with spin and parity $11/2^-$ and $15/2^-$. Similar $11/2^-$ levels (with $M1/E2$ linking transitions) are seen in the neighboring $N=89$ nuclei ^{155}Dy, at 425 keV (current work), and ^{151}Sm at 423.5 keV [18]. The 337- and 422-keV coincident γ rays, previously assigned as depopulating the 887.6-keV $(9/2^-)$ and 550.9 keV $(5/2^-)$ levels [15], are now assigned to the 430.1-keV and 852.2-keV levels in band 9. Band 12 has been observed previously [15] and only the 1141.5-keV level at $17/2^-$ has been added in the present work together with one tentative $21/2^-$ level at 1704 keV. A spin and parity assignment of $9/2^-$ for the level at 333.2 keV is based on the R_{DCO} ratio of the depopulating transition of 239.9 keV ($R_{DCO}=0.4\pm0.1$) feeding the 93.3-keV $7/2^-$ level, and the 291.7-keV γ ray ($R_{DCO}=1.0\pm0.1$) feeding the $5/2^-$, 41.5-keV level. Connecting $M1/E2$ transitions are now established between bands 11 and 12. Additionally, the levels with spin $9/2^-$ and above in both bands decay by $E1$ transitions to levels in band 6.

IV. DISCUSSION

The phenomenon of identical bands (IB's) in nuclei has attracted a great deal of attention (see Ref. [20] for a com-

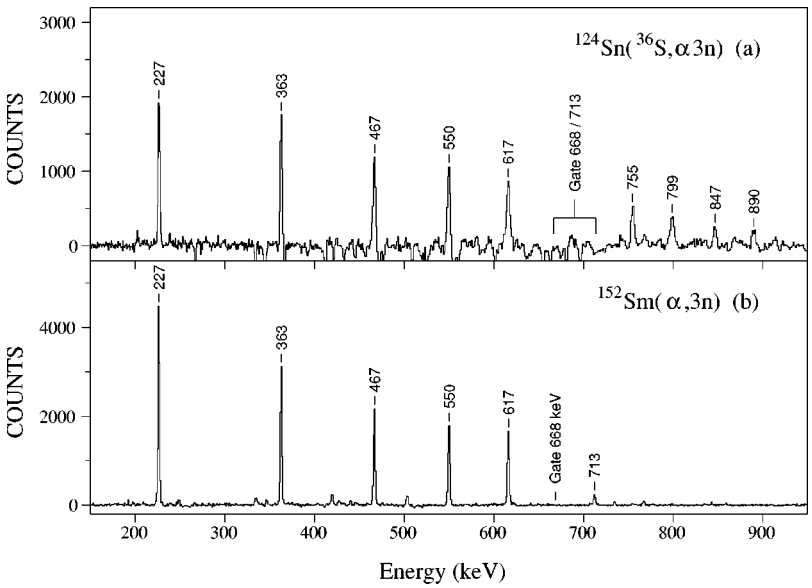

FIG. 3. (a) Spectrum of transitions in triple coincidence with the 668, 713-keV $37/2^+ \rightarrow 33/2^+$, $41/2^+ \rightarrow 37/2^+$ transitions of band 6 ($i_{13/2}$ [660]1/2) from the ^{36}S-beam experiment. (b) Spectrum of transitions in coincidence with the 668-keV $37/2^+ \rightarrow 33/2^+$ transition in band 6 from the α-beam measurement.

prehensive review). In normal-deformed nuclei, IB's have been found at low spin in adjacent even-even and odd-mass nuclei, in pairs of even-even nuclei, and also in single and multiphonon vibrational states [21–26]. Whether these remarkable degeneracies are caused by subtle cancellations among the many parameters which can affect the moment of inertia or by some new physics is still an open question. That said, there is increasing evidence, at least for normal-deformed nuclei at low spins, that the IB's between adjacent even-even and odd-mass nuclei occur because of cancellations between pairing and deformation parameters. A previously unrecognized occurrence of IB's appears for ^{153}Gd and ^{155}Dy where the yrast lines ($\nu i_{13/2}$ bands) of the $N=89$, even-Z nuclei seem to converge to identical transition energies (in keV) (e.g., ^{151}Sm = 235, 374, 478, 561; ^{153}Gd = 227, 363, 467, 550; ^{155}Dy = 227, 363, 464, 544; ^{157}Er = 266, 415, 527, 622; ^{159}Yb = 300, 448, 550, 633, etc.).

The comparison of ^{153}Gd and ^{155}Dy seems particularly interesting for several reasons. First, the similarity of these two nuclei is somewhat surprising considering that these are transitional nuclei and, supposedly, rather soft to polarizing influences, although theoretical calculations, see, for example, Ref. [27], predict the neighboring $N=88$ cores (^{152}Gd and ^{154}Dy) to have very similar deformations. Second, the level structure of ^{155}Dy is known extremely well from our previous and present work with numerous bands built on different Nilsson orbitals that have been delineated together with various vibrational structures built on these orbitals. Thus, it is of interest to compare the correlation of IB's in the two nuclei with regard to the different occupied Nilsson orbitals (instead of just the $i_{13/2}$ yrast bands) and, hence, to learn more about the microscopic details of this phenomenon from the various polarizing tendencies of the different orbitals. In the following sections, the comparison between bands in these $N=89$ nuclei is explored and discussed.

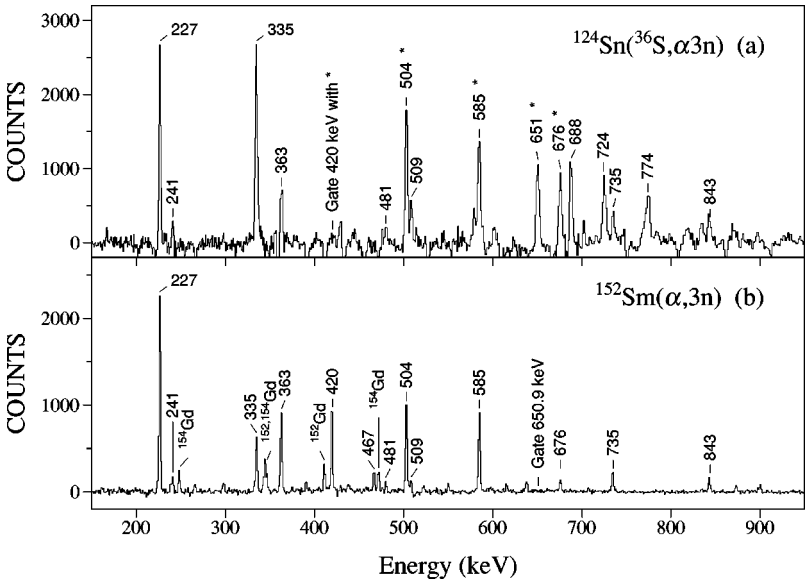

FIG. 4. (a) Spectrum of transitions in triple coincidence with the 419.8-keV $25/2^+ \rightarrow 21/2^+$ transition and other member transitions (*) in band 4 from the ^{36}S-beam measurement. (b) Spectrum of transitions in coincidence with the 650.9-keV $37/2^+ \rightarrow 33/2^+$ transition in band 4 from the α-beam experiment.

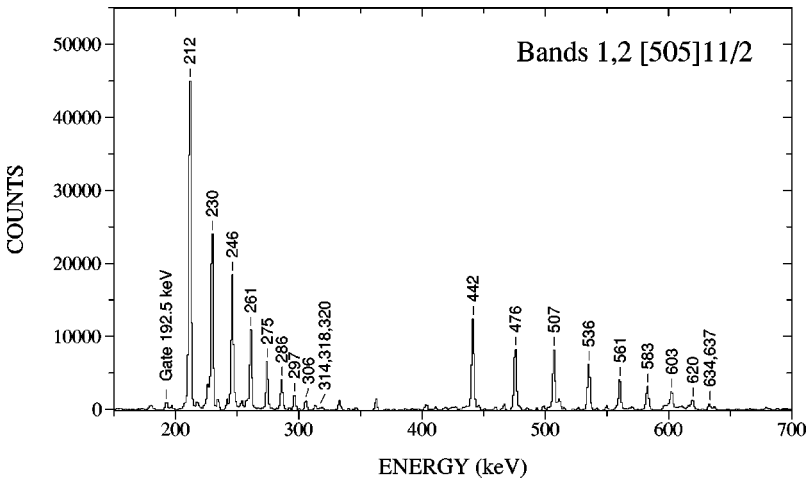

FIG. 5. Spectrum of transitions in bands 1 and 2 ($h_{11/2}[505]11/2$) in coincidence with the 192.5-keV $13/2^- \rightarrow 11/2^-$ transition from the α-beam experiment.

Configuration assignments will be discussed within the framework of the cranked shell model [28–30]. The expected band crossings in the frequency range accessed in these experiments are the first, second, and third $i_{13/2}$ neutron alignments (*AB* [31], *BC* [32,33], and *AD*), and the first $h_{11/2}$ proton alignment A_pB_p [4]. As mentioned previously, it is important to note the existence of low-energy (<2 MeV) vibrational states in the neighboring even-even nuclei [34,35]. Additional rotational sequences may be observed which correspond to the coupling of these vibrations with the one-quasiparticle states.

A. Positive-parity levels

1. Bands 3 and 6

These bands are interpreted as the unfavored and favored signatures of the $i_{13/2}$ [660]1/2 orbital, respectively. These assignments are consistent with the expected large signature splitting characteristic of this low-*K* orbital. As seen in Fig. 6, band 6 shows a smooth gain in alignment starting at $\hbar\omega \sim 0.37$ MeV which is interpreted as the *BC* neutron crossing [36]. Note that the observed interaction strength in the band crossing region has been used as a deformation indicator in the neighboring nuclei [32]. In contrast, a plot of the γ-ray energy differences of the $i_{13/2}$ favored signature bands in ^{157}Er–^{155}Dy in Fig. 7 shows that the level spacing is very much greater in ^{157}Er than in ^{155}Dy or ^{153}Gd. This is a consequence of a smaller deformation in ^{157}Er. The similarity of ^{155}Dy and ^{153}Gd is seen in Fig. 7 for all bands, except band 4 above spin $I=15\hbar$, with $\Delta E_\gamma \leqslant 15$ keV over a $20\hbar$ spin range and a transition-energy range of $E_\gamma \simeq 200-900$ keV. It is perhaps interesting to note that while it is the low-*K* [660]1/2 orbital which is most similar at low spins, it is the high-*K* [505]11/2 orbital that is most different.

2. Band 4

The interpretation for band 4 is not that of a simple one-quasiparticle configuration. The initial alignment ($i_x=5.1$) of this band (Fig. 6) is similar to that of the [660]1/2 band, however, the [660]1/2 orbit is the only one available near the Fermi surface with such high initial alignment. The excitation energy (Fig. 8) of band 4 is approximately 500 keV above the yrast [660]1/2 configuration. This is similar to the excitation energy of beta vibrations in the neighboring even-*N* Gd isotopes (see Fig. 9). The initial levels of band 4 are

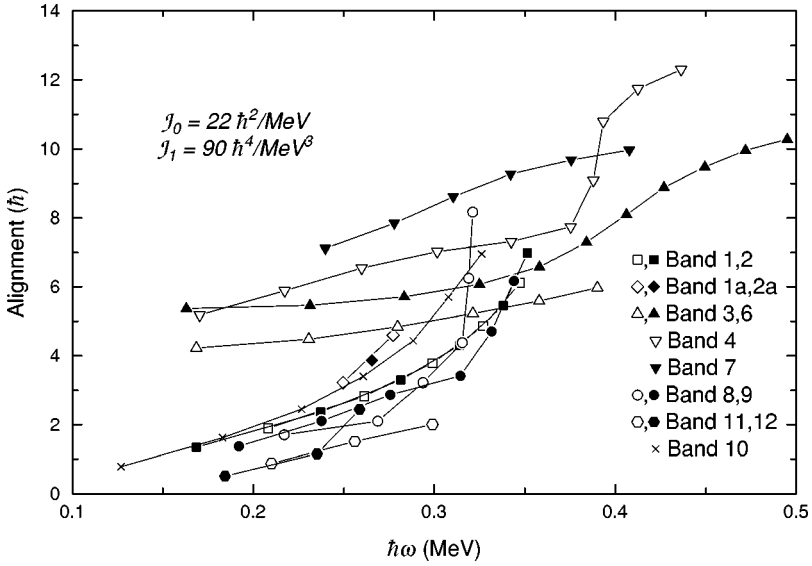

FIG. 6. Experimental alignments for bands in ^{153}Gd. The Harris parameters chosen are $J_0 = 22\ \mathrm{MeV}^{-1}\hbar^2$ and $J_1 = 90\ \mathrm{MeV}^{-3}\hbar^4$.

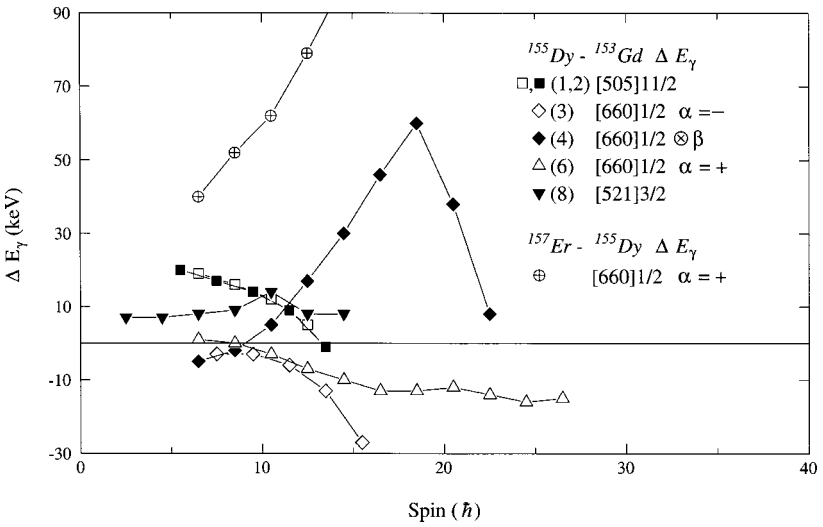

FIG. 7. Energy differences (^{155}Dy-^{153}Gd) between γ-ray transitions for similar structures in ^{153}Gd and ^{155}Dy. Also shown are the energy differences (^{157}Er-^{155}Dy) for the $i_{13/2}$ [660]1/2 yrast band.

then best interpreted as a beta vibration coupled to the $i_{13/2}$ [660]1/2 neutron. Beyond spin $29/2^+$, band 4 experiences at a rotational frequency of $\hbar\omega = 0.32$ MeV (see Fig. 6) a sharper gain in alignment than the [660]1/2 band . This sharp gain in alignment is possibly associated with the energetic proximity to the aligned *ABC* configuration leading to a mixed three-quasiparticle configuration. This behavior appears to be similar to the ''twin backbending'' in ^{154}Gd [32] and ^{156}Dy [4], where the aligned *AB* band crosses both the ground-state band and the beta-vibrational sequence. The present observation in ^{153}Gd is the first case of this kind found in an odd nucleus. Compared with a rigid rotor in Fig. 8, at the highest spins, band 4 approaches and appears as though it may cross the [660]1/2 band beyond the observed levels. What happens at spins higher than those observed here is an intriguing question for future experiments.

3. Band 10

The 212 keV level of band 10 has been assigned to the $d_{3/2}$ [402]3/2 orbital [16,17]. To understand the appearance of this orbital near the Fermi level it must be considered predominantly as a hole state with the extra neutron promoted to one of the $h_{9/2}/f_{7/2}$ negative-parity orbitals. The addition of a neutron in these orbitals causes the nucleus to increase its deformation [1], thus bringing the strongly upsloping [402]3/2 orbital closer to the Fermi level. As for the [505]11/2 bands (1 and 2), band 10 shows a significant smooth gain in alignment near $\hbar\omega = 0.3$ MeV which is attributed to the first $i_{13/2}$ (*AB*) crossing.

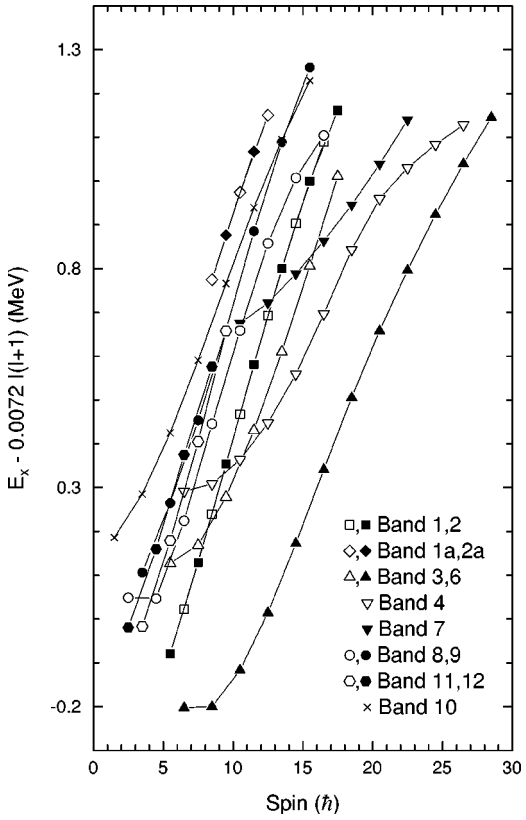

FIG. 8. Excitation energies of levels in ^{153}Gd with a rigid rotor reference subtracted.

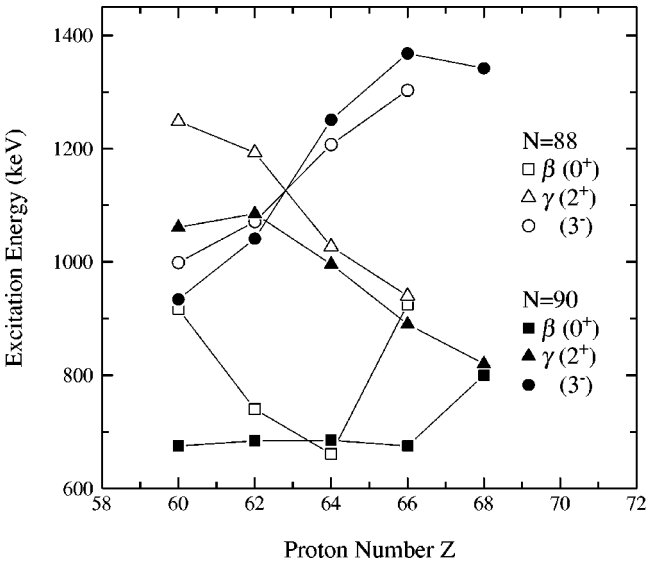

FIG. 9. Excitation energies of the 0^+ (β), 2^+ (γ), and lowest 3^- states in $N=88$, 90 nuclei.

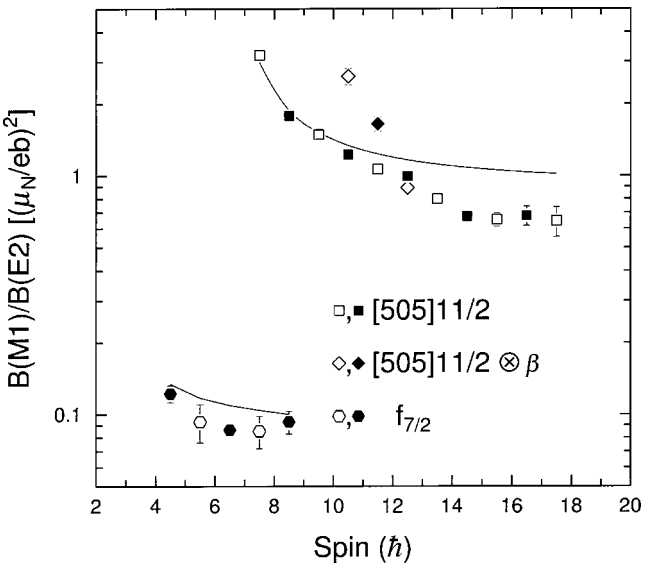

FIG. 10. Experimental and calculated $B(M1)\Delta I = 1/B(E2)\Delta I=2$ ratios for the [505]11/2 (bands 1 and 2, and 1a and 2a) and the $f_{7/2}$ (bands 11 and 12) configurations.

B. Negative-parity levels

1. Bands 1 and 2

Bands 1 and 2 are based on the $h_{11/2}\,[505]11/2^-$ orbital (labeled *X* and *Y* using the convention of Riley *et al.* [4]). The ratio of the $B(M1)/B(E2)$ transition strengths can be deduced from the measurement of the $(I\rightarrow I-1)$ to $(I\rightarrow I-2)$ branching ratios within the signature partner bands by using the expression

$$\frac{B(M1;\ I\rightarrow I-1)}{B(E2;\ I\rightarrow I-2)} = 0.697\ \frac{E_\gamma^5\ (I\rightarrow I-2)}{E_\gamma^3\ (I\rightarrow I-1)}\ \frac{1}{\lambda(1+\delta^2)}\ \left(\frac{\mu_N}{eb}\right)^2, \qquad (1)$$

where the transition energies are in MeV. Figure 10 compares the experimental and calculated $B(M1)/B(E2)$ values for bands 1 and 2, 1a and 2a, and 11 and 12. The theoretical values were obtained using the prescription and standard parameters, of Dönau [37] and Frauendorf [38] (with $\delta=0$). Excellent agreement between the calculations and experiment is found.

2. Bands 1a and 2a

The levels in these bands, like bands 1 and 2, display essentially no signature splitting and are connected by both $\Delta I=1$ and $\Delta I=2$ transitions. Similar excited bands have been observed in ^{151}Sm [18] but no interpretation was proposed. However, these levels (in both nuclei) are too low in excitation energy to correspond to three-quasiparticle bands. The similarity of decay structure and relative energy ($\sim$500 keV) of bands 1a and 2a to bands 1 and 2 suggest that they are most likely associated with a beta vibration coupled to the *X* and *Y* [505]11/2 neutrons. The alignment of these bands, $\sim 1\hbar$ greater than the [505]11/2 bands as seen in Fig. 6, is similar to that of band 4 compared with band 6 (see above discussion for band 4). Furthermore, the $B(M1)/B(E2)$ ratios are similar to those of bands 1 and 2 as can be seen in Fig. 10.

3. Bands 8, 9, 11, and 12

Several problems occur when attempting to assign configurations to the negative-parity bands in the $N=89$ nuclei using the Nilsson model. Weak deformation and the presence of such a large number of low-*K* orbitals near the Fermi surface result in heavily mixed Nilsson configurations that are in turn influenced by Coriolis mixing. Early particle-transfer studies of ^{151}Sm [39], ^{153}Gd [17,40], and ^{155}Dy [41] noted these difficulties. Subsequent application of the particle-rotor model to the nucleus ^{151}Sm [42–44] provided for the first time a consistent description of the observed negative-parity states. A later experiment on ^{153}Gd was performed [15] and good agreement was found between experiment and theory as for ^{151}Sm. Comparison of the experimental data on level spins, energies, and spectroscopic factors showed that the two observed rotational bands (including both signatures) could both be described as $K=3/2$, with one arising from $f_{7/2}$ parentage and the other from $h_{9/2}$ parentage. Two important points came from the calculation. First, the ground-state band is of mainly from $f_{7/2}$ parentage. Second, the lowest $9/2^-$ state is not a member of the ground-state band, but is a member of the $h_{9/2}$ band that is partly decoupled. At that time, a complete level scheme existed for ^{151}Sm, but the data for ^{153}Gd was missing the higher-spin members of the $f_{7/2}$ favored signature. The current data have revealed these missing states at 430.1 keV ($11/2^-$) and 852 keV ($15/2^-$) and excellent agreement is found with the predicted states of Rekstad *et al.* [15] for all bands. Therefore, we will refer to bands 8 and 9 simply as $h_{9/2}$ and bands 11 and 12 as $f_{7/2}$.

4. Band 7

Bands similar to band 7 are seen in other $N=89$ nuclei ^{151}Sm, ^{155}Dy and ^{157}Er. In ^{155}Dy and ^{157}Er these bands have been interpreted [3,45,7] as the three-quasiparticle band *EAB*. However, as shown in Fig. 11, the initial alignments of these bands in all four nuclei are $\sim 7\hbar$. Such an initial alignment is not consistent with a configuration involving aligned *AB* quasiparticles which contribute $\sim 10\hbar$, but no one-quasiparticle configuration exists near the Fermi surface with such large alignment. It has been suggested that this anomalous alignment is caused by mixing with a low-lying octupole-vibrational band [45]. A simple solution is to assume that the lowest-spin members of band 7 are created by the coupling of an octupole phonon to the $i_{13/2}$ band. Such states would have negative parity and, therefore, mix with the aligning three-quasiparticle states in band 8 (see Fig. 2). However, with increasing spin the dominant character changes through mixing with three-quasiparticle states and eventually band 7 is better characterized as the *EAB* band. Similar arguments have been used to explain the evolution of

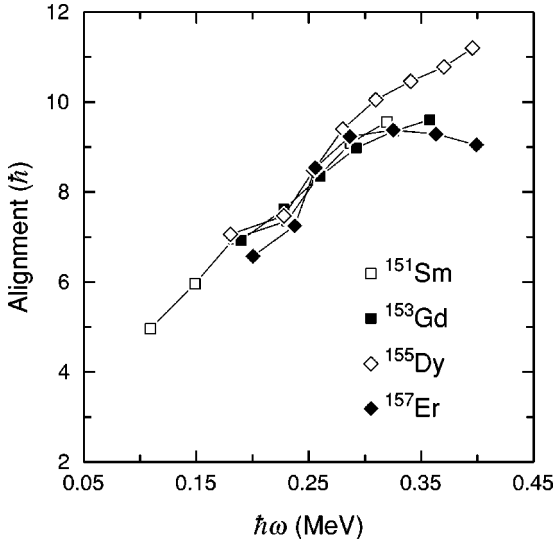

FIG. 11. Experimental alignments of band 7 in ^{153}Gd and its analog in other $N=89$ nuclei.

the octupole band in ^{152}Gd with increasing spin [34] and a theoretical discussion of this evolution can be found in Ref. [46].

Looking at the low-spin members of these ''octupole'' and $h_{9/2}$ bands in more detail, we see a perturbation of the $21/2^-$ level energy occurs in the one-quasiparticle $h_{9/2}$ band in each of the four nuclei ^{151}Sm, ^{153}Gd, ^{155}Dy, and ^{157}Er, which stems from the energetic proximity of the $21/2^-$ states in the two bands. In fact, this perturbation induces a weak decay of the rotational members of the $h_{9/2}$ band in ^{153}Gd and ^{151}Sm to the [660]1/2 band via $E1$ transitions. While compiling the systematics for these $h_{9/2}$ bands in these $N=89$ nuclei, a discrepancy between ^{157}Er and the other $N=89$ nuclei was noticed, namely, the assignment of a 157-keV transition as the $13/2^-\rightarrow 9/2^-$ transition [7,45] in ^{157}Er. In the other $N=89$ nuclei the energy of the transition between these levels is <340 keV. To solve this problem in ^{157}Er, data from a Eurogam ^{114}Cd(^{48}Ca,xn) at a 210 MeV experiment were examined [7]. A solution was found since a new 512-keV $17/2^-\rightarrow 13/2^-$ transition, previously masked by a strong 513-keV transition, was added to the $h_{9/2}$ band in ^{157}Er. Using previously published DCO ratios [7,45], the $N=89$ level systematics, and the multiple $E2$ decay branches, a revised level scheme for these negative-parity bands in ^{157}Er is shown in Fig. 12. The 157-keV transition is reassigned as the $9/2^-\rightarrow 7/2^-$ $M1/E2$ and a new 182-keV transition is assigned as the $9/2^-\rightarrow 5/2^-$ $E2$ transition. These transitions are analogous to the 127- ($M1/E2$) and 178- ($E2$) keV transitions in ^{153}Gd, and the 139- ($M1/E2$) and 186- ($E2$) keV transitions in ^{155}Dy.

V. CONCLUSION

In conclusion, two experiments have been performed to extend considerably the experimental knowledge of excited states in the $N=89$ nucleus ^{153}Gd. Corrections have been made to the previously published level scheme, and new

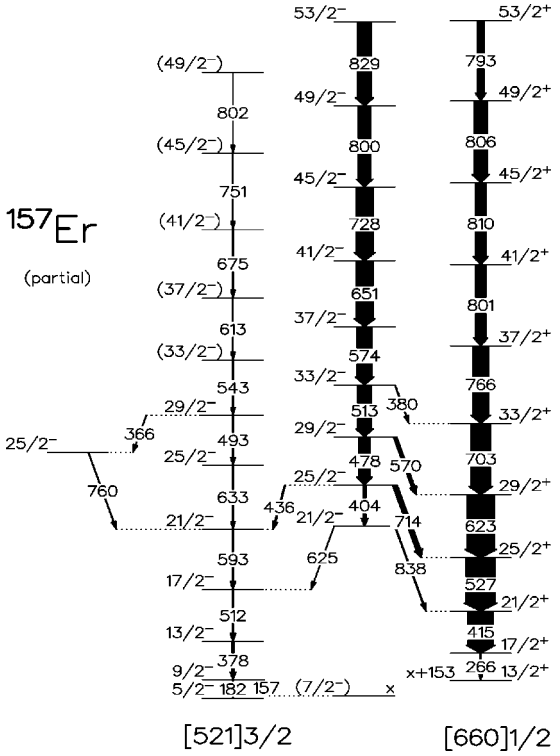

FIG. 12. Revised partial level scheme for ^{157}Er showing the new addition of the 512-keV γ ray ($17/2^-\rightarrow 13/2^-$) to the $h_{9/2}$ band. The excitation energies of the levels are unknown. Note that the $13/2^+$ level is now at an excitation energy $+153$ keV relative to the proposed ($7/2^-$) level. See text for details.

band structures have been observed. The present rotational structures in ^{153}Gd have been interpreted using the cranked shell model. Strong similarities to ^{155}Dy in terms of isospectral bands have been observed and arguments have been put forth indicating that these two nuclei, in contrast to other $N=89$ nuclei, have similar deformations. The alignment of the second alignable pair of $i_{13/2}$ neutrons (BC) is observed near $\hbar\omega=0.38$ MeV. Evidence is also found, for the first time in an odd-A nucleus in this region, that the aligned three-quasiparticle ABC configuration crosses the $A\otimes$ beta-vibration band in an analogous manner to that of the ''twin backbending'' observed in neighboring even-even nuclei. In addition, this systematic study of several $N=89$ nuclei has led to a correction to the low-spin level scheme of ^{157}Er.

ACKNOWLEDGMENTS

Special thanks go to D. C. Radford, R. M. MacLeod, and H. Q. Jin for their software support, and to R. Darlington for help with the targets. We are grateful to J. X. Saladin whose loan of the University of Pittsburgh detectors and electronics made the FSU-Pitt detector array possible. Support for this work was provided by the U.S. Department of Energy Nuclear Physics Division under Contract No. W-31-109-ENG-38, the National Science Foundation, the State of Florida, and the United Kingdom Council for the Engineering and Physical Sciences Research Council.

[1] R.F. Casten, D.D. Warner, D.S. Brenner, and R.L. Gill Phys. Rev. Lett. **47**, 1433 (1981).
[2] W.C. Ma, M.A. Quader, I. Ahmad, P.J. Daly, B.K. Dichtes, M. Drigert, H. Emling, U. Garg, Z.W. Grabowski, R. Holtzmann, R.V.F. Janssens, T.L. Khoo, M. Piiparinen, W.H. Trzaska, and T.F. Wang, Phys. Rev. Lett. **61**, 46 (1988).
[3] R. Vlastou, C.T. Papadopoulos, M. Serris, C.A. Kalfas, N. Fotiades, S. Harissopulos, S. Kossionides, J.F. Sharpey-Schafer, E.S. Paul, P.D. Forsyth, P.J. Nolan, N.D. Ward, M.A. Riley, J. Simpson, J.C. Lisle, P.M. Walker, M. Guttormsen, and J. Rekstad, Nucl. Phys. **A580**, 133 (1994).
[4] M.A. Riley, J. Simpson, J.F. Sharpey-Schafer, J.R. Cresswell, H.W. Cranmer-Gordon, P.D. Forsyth, D. Howe, A.H. Nelson, P.J. Nolan, P.J. Smith, N.J. Ward, J.C. Lisle, E. Paul, and P.M. Walker, Nucl. Phys. **A486**, 456 (1988).
[5] F.G. Kondev, M.A. Riley, R.V.F. Janssens, J. Simpson, A.V. Afanasjev, I. Ragnarsson, I. Ahmad, D.J. Blumenthal, T.B. Brown, M.P. Carpenter, P. Fallon, S.M. Fischer, G. Hackman, D.J. Hartley, C.A. Kalfas, T.L. Khoo, T. Lauritsen, W.C. Ma, D. Nisius, J.F. Sharpey-Schafer, and P.G. Varmette, Phys. Lett. B **437**, 35 (1998).
[6] J. Simpson, M.A. Riley, S.J. Gale, J.F. Sharpey-Schafer, M.A. Bentley, A.M. Bruce, R. Chapman, R.M. Clark, S. Clarke, J. Copnell, D.M. Cullen, P. Fallon, A. Fitzpatrick, P.D. Forsyth, S.J. Freeman, P.M. Jones, M.J. Joyce, F. Liden, J.C. Lisle, A.O. Macchiavelli, A.G. Smith, J.F. Smith, J. Sweeney, D.M. Thompson, S. Warburton, J.N. Wilson, T. Bengtsson, and I. Ragnarsson, Phys. Lett. B **327**, 187 (1994).
[7] S.J. Gale, J. Simpson, M.A. Riley, J.F. Sharpey-Schafer, E.S. Paul, M.A. Bentley, A.M. Bruce, R. Chapman, R.M. Clark, S. Clarke, J. Copnell, D.M. Cullen, P. Fallon, A. Fitzpatrick, P.D. Forsyth, S.J. Freeman, P.M. Jones, M.J. Joyce, F. Liden, J.C. Lisle, A.O. Macchiavelli, A.G. Smith, J.F. Smith, J Sweeney, D.M. Thompson, S. Warburton, J.N. Wilson, and I. Ragnarsson, J. Phys. G **21**, 193 (1995).
[8] T. Byrski, F.A. Beck, J.C. Merdinger, A. Nourreddine, H.W. Cranmer-Gordon, D.V. Elenkov, D. Howe, P.D. Forsyth, M.A. Riley, J.F. Sharpey-Schafer, J. Simpson, J. Dudek, and W. Nazarewicz, Nucl. Phys. **A474**, 193 (1987).
[9] *Gammasphere, A National Gamma-ray Facility*, edited by M.A. Deleplanque and R.M. Diamond (Lawrence Berkeley Laboratory, Berkeley, CA, 1988); I.Y. Lee, Nucl. Phys. **A520**, 641c (1990); R.V.F. Janssens and F.S. Stephens, Nucl. Phys. News **6**, 9 (1996).
[10] S.L. Tabor, M.A. Riley, J. Döring, P.D. Cottle, R. Books, T. Glasmacher, J.W. Holcomb, J. Hutchins, G.D. Johns, T.D. Johnson, T. Petters, O. Tekyi-Mensah, P.C. Womble, L. Wright, and J.X. Saladin, Nucl. Instrum. Methods Phys. Res. B **79**, 821 (1993).
[11] D. Radford, Nucl. Instrum. Methods Phys. Res. A **361**, 297 (1995).
[12] T.B. Brown *et al.* (unpublished).
[13] I. Rezanka, F.M. Bernthal, J.O. Rasmussen, R. Stokstad, I. Fraser, J. Greenberg, and D.A. Bromley, Nucl. Phys. **A179**, 51 (1972).
[14] G. Løvhøiden, S.A. Hjorth, H. Ryde, and L. Harms-Ringdahl, Nucl. Phys. **A181**, 589 (1972)
[15] J. Rekstad, P. Boe, A. Henriquez, R. Oyan, M. Guttormsen, T. Engeland, and G. Løvhøiden, Nucl. Phys. **A371**, 364 (1981).
[16] P.O. Tjøm and B. Elbek, Mat. Fys. Medd. K. Dan. Vidensk. Selsk. **36**, No. 8 (1967).
[17] G. Løvhøide and D.G. Burke, Can. J. Phys. **51**, 2354 (1973).
[18] M.K. Khan, W.J. Vermeer, W. Urban, J.B. Fitzgerald, A.S. Mowbray, B.J. Varley, J.L. Durell, and W.R. Phillips, Nucl. Phys. **A567**, 49 (1994).
[19] R.B. Firestone, in *Table of Isotopes*, 8th ed., edited by V.S. Shirley (Wiley, New York, 1996).
[20] C. Baktash, B. Haas, and W. Nazarewicz, Annu. Rev. Nucl. Part. Sci. **45**, 1 (1995).
[21] C. Baktash, J.D. Garrett, D.F. Winchell, and A. Smith, Phys. Rev. Lett. **69**, 1500 (1992).
[22] J.-Y. Zhang and L.L. Riedinger, Phys. Rev. Lett. **69**, 3448 (1992).
[23] I. Ahmad *et al.*, Nucl. Phys. **A513**, 125 (1991).
[24] R.F. Casten, N.V. Zamfir, P. von Brentano, and W.-T. Chou, Phys. Rev. C **45**, R1413 (1992).
[25] J.-Y. Zhang, R.F. Casten, W.-T. Chou, D.S. Brenner, N.V. Zamfir, and P. von Brentano, Phys. Rev. Lett. **69**, 1160 (1992).
[26] X. Wu *et al.*, Phys. Lett. B **316**, 235 (1993).
[27] W. Nazarewicz, M.A. Riley, and J.D. Garrett, Nucl. Phys. **A512**, 61 (1990).
[28] R. Bengtsson and S. Frauendorf, Nucl. Phys. **A314**, 27 (1979).
[29] R. Bengtsson and S. Frauendorf, Nucl. Phys. **A327**, 139 (1979).
[30] R. Bengtsson, S. Frauendorf, and F.R. May, At. Data Nucl. Data Tables **35**, 15 (1986).
[31] J. Simpson, M.A. Riley, A. Alderson, M.A. Bentley, A.M. Bruce, D.M. Cullen, P. Fallon, F. Hanna, and L. Walker, J. Phys. G **17**, 511 (1991).
[32] J.D. Morrison, J. Simpson, M.A. Riley, H.W. Cranmer-Gordon, P.D. Forsyth, D. Howe, and J.F. Sharpey-Schafer, J. Phys. G **15**, 1871 (1989).
[33] D.J. Hartley, J.L. Allen, T.B. Brown, F.G. Kondev, J. Pfohl, M.A. Riley, S.M. Fischer, R.V.F. Janssens, D.T. Nisius, P. Fallon, W.C. Ma, and J. Simpson, Phys. Rev. C **59**, 1171 (1999).
[34] M. Guttormsen, J. Rekstad, and L.L. Riedinger, Phys. Scr. **22**, 210 (1980).
[35] D.C. Sousa, L.L. Riedinger, E.G. Funk, and J.W. Mihelich, Nucl. Phys. **A238**, 365 (1975).
[36] R. Bengtsson, S. Frauendorf, and F.R. May, At. Data Nucl. Data Tables **35**, 15 (1986).
[37] F. Dönau, Nucl. Phys. **A471**, 469 (1987).
[38] S. Frauendorf, Phys. Lett. **100B**, 219 (1981).
[39] D.E. Nelson, D.G. Burke, J.C. Waddington, and W.B. Cook, Can. J. Phys. **51**, 2000 (1973).
[40] G. Løvhøiden, D.G. Burke, and J.C. Waddington, Can. J. Phys. **51**, 1369 (1973).
[41] O. Straume, D.G. Burke, and T.F. Thorsteinsen, Can. J. Phys. **54**, 1258 (1976).
[42] M. Guttormsen, E. Osnes, J. Rekstad, G. Løvhøiden, and O. Straume, Nucl. Phys. **A298**, 122 (1978).
[43] R. Katajanheimo and E. Hammarén, Phys. Scr. **19**, 497 (1979).
[44] S.A. Hjort and W. Klamra, Z. Phys. A **283**, 287 (1977).
[45] J. Simpson, M.A. Riley, J.F. Sharpey-Schafer, J.C. Bacelar, A.P. Cook, J.R. Cresswell, D.V. Elenkov, P.D. Forsyth, G.B. Hagemann, B. Herskind, A. Holm, D. Howe, and B.M. Nyako, J. Phys. G **15**, 643 (1989).
[46] P. Vogel, Phys. Lett. **60B**, 431 (1976).